Nutrient uptake by chemotactic bacteria in presence of rising oil drops

Nikhil Desai

School of Mechanical Engineering, Purdue University, West Lafayette, Indiana, USA, 47907.

Sadegh Dabiri

School of Mechanical Engineering, Purdue University, West Lafayette, Indiana, USA, 47907.

Department of Agricultural and Biological Engineering, Purdue University, West Lafayette, Indiana, USA, 47907.

Arezoo M. Ardekani*

School of Mechanical Engineering, Purdue University, West Lafayette, Indiana, USA, 47907.

Abstract

We investigate the consumption of a dissolved chemoeffector by model bacteria, in a flow generated by buoyancy driven rise of oil drops. Our aim is to quantify the differences in the rate of consumption by motile and non-motile bacteria. We employ direct numerical simulations to resolve the multiphase flow, chemoeffector transport, and bacteria transport in a swarm of rising oil drops. Our simulations indicate that chemotaxis enables motile bacteria to consume the chemoeffector at rates that can be ≈45% faster than their non-motile counterparts. We find that the chemotactic advantage depends most acutely on the bacteria's swimming speed, and on their sensitivity toward gradients in chemoeffector concentration. Furthermore, our results reveal that chemotactic advantage reduces monotonically with an increase in the diameter of the drops, while it varies non-trivially with the volume fraction of the drops.

*Corresponding author
Email address: ardekani@purdue.edu (Arezoo M. Ardekani)

Keywords: Biodegradation | Swarm of oil drops | Motile bacteria

1. Introduction

Subsurface hydrocarbon (HC) spills/leaks−both natural and anthropogenic−are a major source of carbon and energy for a plethora of marine microorganisms [1]. In fact, the role of methanotrophs in degrading methane in the Deepwater Horizon spill in 2010 is well documented [2, 3, 4]. A major portion of this degradation occurred in the presence of a rising swarm of oil drops, i.e., in an inherently unsteady flow environment consisting of at least two distinct fluid phases [5]. Similarly, it is expected that the many *soluble* HCs being leaked into the oceans are also consumed by marine bacteria under the influence of flows that are driven by buoyancy of the *insoluble* oil components (e.g., high-molecular-weight aliphatic hydrocarbons). These flows result in significant three dimensional velocity fluctuations (called 'pseudo-turbulence') due to the hydrodynamic interactions between the oil drops [6, 7, 8, 9]. The velocity fluctuations in turn drive dispersion of the dissolved HCs via combined diffusive and convective transport. Therefore, pseudo-turbulence ensures that not only is the fluid medium in a state of agitation, but that any concentrated 'patches' of dissolved HCs are being continuously stirred (dispersed into thinner or smaller patches, resulting in enhanced HC/nutrient gradients) and mixed (homogenized due to fluid flow and nutrient diffusion).

The aforementioned processes are expected to create a fundamental difference in the nutrient uptake by motile bacteria, as compared to that by the non-motile ones. Central to understanding this difference is a well studied phenotype of bacteria called chemotaxis [10]: the 'gradient sensing ability' of a bacterium that allows it to alter its swimming strategy in order to reside in regions of high (low) concentrations of desired (undesired) chemical species called chemoattractants (chemorepellants). The pseudo-turbulence engenders nutrient gradients and drives chemotactic motion of motile microbes. For example, methanotrophic bacteria like *Methylomonas* can chemotax toward methane-rich

regions in a HC plume [2]. This directed motion exists only for motile bacteria, which hints at the advantage that they might have over their non-motile counterparts. However, the extent to which chemotaxis can be beneficial is not known *a priori*, and requires detailed investigation of the transport phenomena involved. The way in which these organisms consume nutrients relative to each other, and the factors that influence this competition are unclear, and subject to multifarious bio-physical interactions. In the present work, we unravel the results of these interactions, through mathematical models and direct numerical simulations (DNS).

Our problem statement entails modeling the consumption (uptake) of a dissolved chemoattractant (nutrient) by model bacteria−both motile and non-motile−in a swarm of oil drops rising through a column of fluid. The chemoattractant is present in a patch that gets de-localized into thinner 'strands' due to the fluid flow induced by the drops (see Fig. 1 (a) and (b)). We investigate the interaction of physical/flow characteristics (oil drop diameter and volume fraction) with biological characteristics (time scale of nutrient consumption by bacteria, sensitivity to nutrient gradients, swimming speed), and the resulting effect on the competitive consumption of the available nutrient. Our aim is to ascertain and quantify the 'chemotactic advantage', i.e., the difference between the consumption rates by motile and non-motile bacteria, that arises due to chemotactic ability of the former [11]. An important physical parameter that governs the consumption dynamics is the molecular diffusivity of the nutrient, which eventually smears out any heterogeneities in the nutrient distribution. Nutrient gradients developed by pseudo-turbulence disappear quickly, or slowly, depending on whether the nutrient diffusivity is high, or low, respectively. The typical diffusivity values for nutrients range from 10^{-5} to 10^{-8} cm^2/s [12], which is three orders of magnitude smaller than the momentum diffusivity of water (10^{-2} cm^2/s). A fully resolved DNS for the nutrient distribution with such small diffusivities is very expensive from a computational perspective. This forces us to choose a larger nutrient diffusivity in our simulations: 5×10^{-4} cm^2/s. Thus, the quantification of the chemotactic advantage

presented in this paper is conservative due to this choice of nutrient diffusivity. The results presented improve our understanding about the consumption of soluble nutrients in sub-surface hydrocarbon plumes. In the Appendix of our paper, we comment on the sensitivity of the results to the nutrient diffusivity and discuss the possible changes that could transpire for more realistic diffusivity values. Although we are motivated by sub-surface HC degradation, we point out that our study can be easily tailored−by merely changing the values of the dimensionless parameters−to simulate chemotaxis in situations involving chemoeffector/nutrient dispersion in other multi-phase flows. In the next Section, we describe our mathematical model and the governing equations in detail.

2. Mathematical Model

We numerically solve the equations governing multi-phase flows, i.e., the continuity equation and the Navier-Stokes equation:

$$\nabla \cdot \mathbf{u} = 0, \tag{1}$$

$$\begin{aligned} \frac{\partial \mathbf{u}}{\partial t} + \nabla \cdot \mathbf{u}\mathbf{u} = -\frac{1}{\rho}\nabla p + \left(1 - \frac{\rho_0}{\rho}\right)\mathbf{g} + \frac{1}{\rho}\nabla \cdot (2\mu \mathbf{E}) \\ + \frac{1}{\rho}\int_{\partial V} \sigma \kappa' \mathbf{n}' \delta^{\beta}\left(\mathbf{x} - \mathbf{x}'\right) dA', \end{aligned} \tag{2}$$

where $\mathbf{u}(x,\ y,\ z,\ t)$ is the fluid velocity field, t is the time, p is the fluid pressure, ρ and μ are the density and viscosity of the fluid, respectively, ρ_0 is the average density of the oil-water system, and σ is the surface tension between oil and water. $\mathbf{E}$ is the rate of strain tensor, defined as $\mathbf{E} = \frac{1}{2}\left(\nabla \mathbf{u} + \nabla \mathbf{u}^{\mathrm{T}}\right)$, with $^{\mathrm{T}}$ denoting the transpose operator acting on the velocity gradient tensor $\nabla \mathbf{u}$. Equation 1 is the condition for incompressibility of a fluid and equation 2 is a differential form of the conservation of fluid momentum. The last term in equation 2 is the contribution of surface tension forces on the fluid flow, with the area integral carried out over all points on the oil-water interface ∂V; $\mathbf{x}$ is

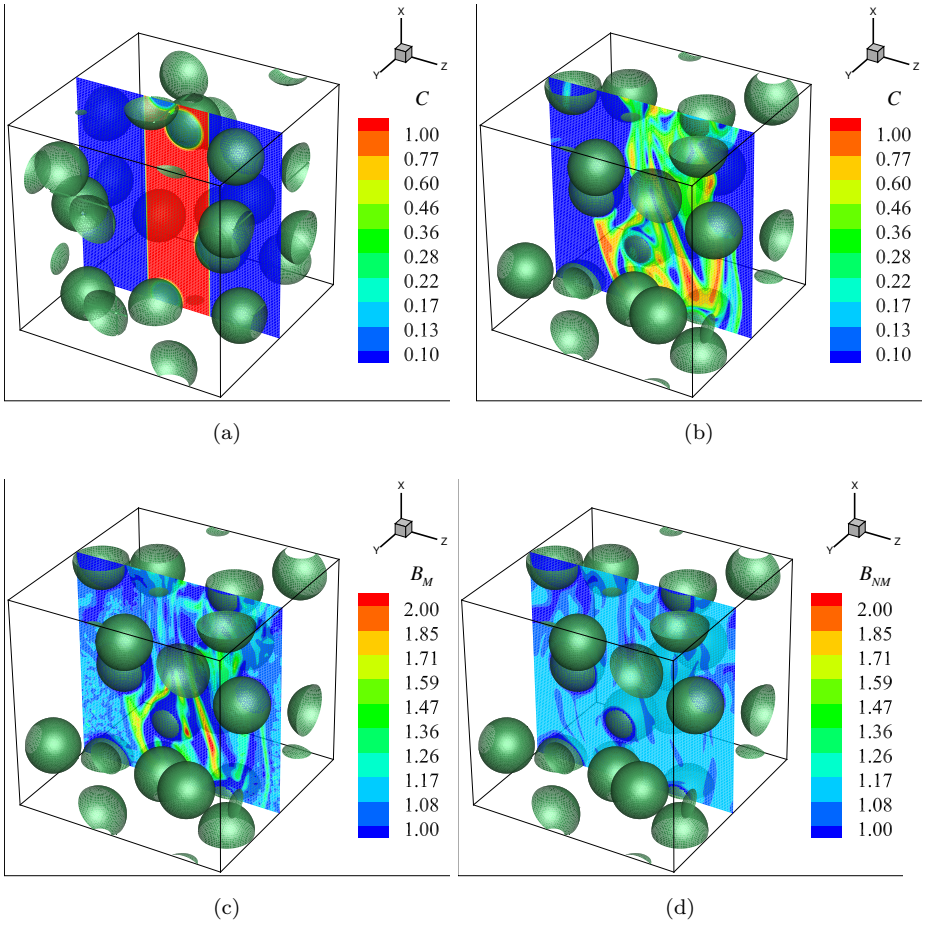

Figure 1: (a) The initial distribution of the chemoattractant/nutrient. (b) The distribution of the nutrient after some time has elapsed in the simulations. (c) The distribution of the motile bacteria at the same instant of time as in (b). Notice higher concentrations of motile bacteria B_M in the nutrient-rich regions, due to chemotaxis. (d) The distribution of the non-motile bacteria at the same instant of time as in (b). Note that the distribution of the non-motile bacteria remains more or less uniform, as there is no bias in their motion.

the point in the fluid domain where we want to evaluate the fluid velocity, κ' is the mean curvature, and $\mathbf{n}'$ is the outward pointing unit vector normal to the interface at the *interface* point $\mathbf{x}'$, and δ^β is the three-dimensional Dirac-delta function [13, 14]. The interface corresponds to the surface of mono-disperse drops of diameter d, density ρ_g and viscosity μ_g, where the subscript g indicates that the desired properties are of the dispersed phase (in our case, an insoluble oil drop). The fluid flow is governed by the Eötvos number $Eo = \frac{\rho_f g d^2}{\sigma}$ (a measure of the relative importance of the buoyancy and surface tension forces), and the Galileo number $Ga = \frac{\rho_f^2 g d^3}{\mu_f^2}$ (a measure of the relative importance of the inertial and viscous forces), where the subscript f indicates that the desired properties of the carrier phase (in our case, water) are being used. The $-(\rho_0/\rho)\mathbf{g}$ term in equation 2 is a force that prevents free fall of the fluid and ensures zero momentum flux through the boundaries of our computational domain [6]. The bacteria−both motile (B_M) and non-motile (B_{NM})−are modeled as a continuum, being transported according to the following advection-diffusion equations:

$$\frac{\partial B_M}{\partial t} + \nabla \cdot \left(\left(\mathbf{u} + V_s \mathbf{p} \right) B_M \right) = \nabla \cdot \left(D_b \nabla B_M \right), \tag{3}$$

$$\frac{d\mathbf{p}}{dt} = \frac{1}{2}\boldsymbol{\omega} \times \mathbf{p} + \frac{1}{\beta_C} \left(\mathbf{I} - \mathbf{pp} \right) \cdot \nabla C, \tag{4}$$

$$\frac{\partial B_{NM}}{\partial t} + \nabla \cdot \left(B_{NM} \mathbf{u} \right) = 0. \tag{5}$$

The non-motile species act as mere tracers that follow the fluid flow, while the motile bacteria have an additional chemotaxis driven velocity $V_s\mathbf{p}$ with respect to the fluid (equation 3). In addition to deterministic swimming, the motile bacteria can also diffuse with diffusivity D_b. This diffusion is indicative of the stochastic nature of bacterial motion. Equation 4−solved only in case of the motile species−is an expression for time evolution of the swimming orientation $\mathbf{p}$, modified to include the effects of external nutrient gradients. The first term on the right hand side is the influence of the background vorticity $\boldsymbol{\omega}$. In

addition to the vorticity, the background strain rate $\mathbf{E}$ also affects the swimming orientation, but only if the bacteria are elongated. As a first approximation, we neglect this latter effect, and assume the bacteria to be nearly spherical in shape. The chemotactic bias in the swimming direction is introduced through the second term on the right hand side of equation 4, which models the effect of an external nutrient gradient (∇C, C being the concentration of the nutrient) on the rate of change of swimming orientation. β_C is the inverse of the chemotactic sensitivity, which determines the relative importance of steering by external chemical gradients as compared to that by external vorticity. In their present form, equations 3 and 4 assume that all cells around a differential volume δV at position $\mathbf{x}$ are oriented along the same direction $\mathbf{p}$. This is a strong assumption, but it adds considerable simplicity to our numerical simulations. A more complete description would require us to couple our multi-phase DNS procedure with a transport equation for the probability distribution $\psi(\mathbf{x}, \mathbf{p}, t)$ of the bacterial positions and orientations, and then perform appropriate averaging to fully incorporate the effects of randomness in swimming orientations in equation 3 (see [15]). This will increase the dimensionality of the system from three to five, and together with the front-tracking method used to fully resolve the evolution of oil-water interface, render the problem computationally unwieldy. A justification of our method is that re-orientations due to flow, and particularly chemotaxis, are strong enough to ensure rapid correction in the swimming direction, over the smallest length scale in our system (≈ 0.03 mm). Therefore, we use the present formulation and integrate equation 4 at each time step and position, instead of using averaged 'equilibrium' values of the vector $\mathbf{p}$ (see a similar method in the context of gyrotaxis, first proposed by Pedley, Hill and Kessler [16], and recently solved numerically by Karimi and Ardekani in the context of gyrotaxis in stratified media [17]). In addition, equation 4 does not contain any rotary diffusive terms, i.e., random, smooth changes in the swimming direction of the bacterium. We chose to neglect this effect based on a simple scaling analysis, towards which we first re-write equation 4, with the inclusion of a random orientation de-correlation due to the rotary diffusivity

D_R:

$$d\mathbf{p} = \left[\frac{1}{2}\omega \times \mathbf{p} + \frac{1}{\beta_C}\left(\mathbf{I} - \mathbf{pp}\right) \cdot \nabla C\right] dt + \left[\sqrt{4D_R}\boldsymbol{\eta}_R \times \mathbf{p}\right] dt, \tag{6}$$

where the rotary diffusion is modeled via a Gaussian white-noise on the unit sphere, $\boldsymbol{\eta}_R$. The vorticity scales as $|\boldsymbol{\omega}| \approx \sqrt{g/d} \approx 44\ \mathrm{s}^{-1}$ to $86\ \mathrm{s}^{-1}$, based on the typical values given in Table 1. In comparison, the orientation change due to a rotary diffusivity value $D_R = 0.035$ to $0.45\ \mathrm{rad}^2/\mathrm{s}$ amounts to $\approx \sqrt{4D_R} \cdot O(1)$ $\mathrm{s}^{-1/2} \approx 0.42\ \mathrm{s}^{-1}$ to $1.34\ \mathrm{s}^{-1}$. Thus, as long as there exists a sufficiently strong background flow, we can safely neglect the effect of rotary diffusion on the bacterial orientation. Fig. 9 in the Appendix shows the difference in the results between the instance that considers rotary diffusivity, and one that does not; clearly, the difference is imperceptible. Note that the use of a deterministic, continuum formulation for chemotaxis, as opposed to the classic run-and-tumble formulation, is justified based on the ratio of the characteristic length scale l_{ref} of our problem ($l_{ref} \equiv$ drop diameter $d \approx$1 mm) to the typical run length l_{run} of marine bacteria (≈ 0.05 mm) being much greater than unity [18, 19]. In such large length scale systems, we can say that equation 4 captures the average reorientation tendency of a chemotactic swimmer in response to chemical cues and ambient flows [20]. It can be thought of as a 'chemotactic torque', or a means to the 'spatial sensing' of nutrient gradients, which is indeed found in some species of microorganisms [21, 22]. Similar models have been used in the absence [23, 24] and presence [25] of external fluid flows to explain phenomena like micro-swimmer clustering and aerotaxis-induced bioconvection plumes, respectively. Lushi *et al.* have performed a study highlighting the similarities between the present model and the run-and-tumble model, in the context of stability and collective motion of auto-chemotactic suspensions [26]. The chemoeffector distribution, $C\left(\mathbf{x}, t\right)$, is governed by the scalar transport equation with a sink term:

$$\frac{\partial C}{\partial t} + \nabla \cdot (C\mathbf{u}) = \nabla \cdot (D_m \nabla C) - \alpha_C B_M C - \alpha_C B_{NM} C, \tag{7}$$

where D_m is the diffusivity of nutrient in water and α_C is a constant which quantifies the nutrient uptake rate by the bacteria. The last two terms on the

right hand side of equation 7 are the reductions in the nutrient concentration due to uptake by the motile and non-motile species, respectively. It is postulated that chemotactic species will 'climb up' the gradients, and as a result, will consume higher concentrations. Since our study is motivated by the extent of consumption, the instantaneous motility benefit is defined as the volume averaged difference between the rates of consumption by the motile and the non-motile species, i.e., motility benefit $\Delta U(t) = \dot{C}_M - \dot{C}_{NM}$ [27], where

$$\dot{C} = \frac{\int\limits_V \alpha_C B C dV}{\int\limits_V dV}, \tag{8}$$

and $B = B_M$ and B_{NM}, for motile and non-motile species, respectively. A benefit due to motility exists only if $\dot{C}_M > \dot{C}_{NM}$. In our results, we normalize $\Delta U(t)$ by the quantity $\alpha_C B_0 C_0$−where B_0 is a baseline number density and C_0 is a baseline nutrient concentration−which has the units μM/s, and signifies a reference consumption rate. In addition to the normalized motility benefit $\Delta \bar{U} = \Delta U/(\alpha_C B_0 C_0)$, we present a measure of the relative rates of consumption by motile and non-motile bacteria, called the 'chemotactic amplification factor' R_U [27]:

$$R_U = \frac{\dot{C}_M + \dot{C}_{NM}}{2\dot{C}_{NM}}, \tag{9}$$

It is clear from the definition that R_U compares the rate of consumption in a region inhabited by both motile and non-motile species, with the scenario where all consumption is assumed to be done by non-motile species alone. It quantifies enhancement in the total uptake rate by a bacterial population due to the chemotactic species. This definition is particularly useful in assessing the chemotactic advantage when the nutrient availability is very low.

We use the finite-volume method on a uniform, structured, staggered grid, combined with the projection method to solve equations 1 and 2 [28]; and track the interface using the front-tracking method [13, 14]. The validation of the front-tracking method being used in this article can be seen in previous publications by the authors [8, 29]. All terms in equation 2 are discretized explicitly using the QUICK scheme for the convective terms [30], central differences for

diffusive terms and front-tracking, with second order accurate representation for δ^β [31], for the surface tension contributions. Equations 3, 5 and 7 are also solved explicitly using the finite-volume method, with convective terms discretized using a fifth order accurate WENO scheme [32] and diffusive terms discretized using central differences. A second order accurate predictor-corrector scheme is employed for all time-integrations. The magnitude of $\mathbf{p}$ is preserved at unity by using a post-stabilization approach used in ref. [17] and detailed in ref. [33].

The initial condition for the fluid-velocity is obtained as the statistically steady-state for a rising swarm of drops [6, 7]. The time evolution of the fluctuation Reynolds number for the various background fluid-flows in the simulations is shown in Fig. 2; while other quantities pertaining to the pseudo-turbulence are detailed in Table 1. It is interesting to note that the energy dissipation rates generated by rising oil drops$-O(10^{-3})$ W/kg$-$are at least 3 orders of magnitude higher than those corresponding to 'relatively strong' marine turbulence ($\sim 10^{-6}$ W/kg) [34]. This allows us to neglect the effects of marine turbulence, and focus solely on the hydrodynamic interactions between rising drops, in our simulations. The initial nutrient-rich region is in the form of a cylinder placed centrally (see Fig. 1), occupying $\approx 8\%$ of the domain volume and with its axis along the direction $\mathbf{g}/\left|\mathbf{g}\right|$. We note that we have also carried out investigations for different initial shapes of the nutrient-rich region, i.e., for (i) a cylindrical shape perpendicular to the direction of ascent (along the y axis in Fig. 1), and, (ii) a spherical shape of same volume as the cylinder (see Fig. 11 in the Appendix and the accompanying discussion). The nutrient concentration inside the drops is set to zero. The concentration of the motile and non-motile bacteria is uniform everywhere, except inside the drops (where it is set to zero). Note that the equation 5, for the evolution of non-motile bacteria does not have any diffusivity, but there exists some numerical diffusion. We do not expect significant clustering of the non-motile bacteria to take place. This is because of the initially uniform distribution of B_{NM}, combined with absence of a term with non-zero divergence in the convective flux of B_{NM} (see the explanations of microorganism clustering based on the divergence of their velocities, as given in

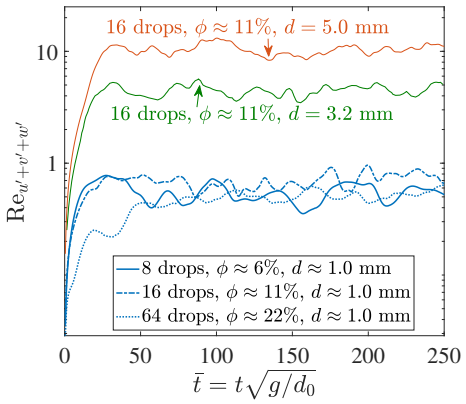

Figure 2: (Color online) Time evolution of the fluctuation Reynolds numbers $\mathrm{Re}_{u'+v'+w'}$ of the drops in the simulations; see the Appendix and the ref. [6, 7] for the definition of the drop fluctuation Reynolds number. The statistical steady states can be easily identified in all 5 cases (at $\bar{t} \approx 50$), the background flow-fields (and drop positions) at these instants are used as the initial condition for the fluid velocity $\mathbf{u}(t = 0)$ in the simulations that are performed to ascertain the chemotactic advantage.

ref. [35]). Thus, $B_{NM}(\mathbf{x}, t)$ is expected to be $\approx B_0$ everywhere in the domain. In our simulations, the value of $|B_{NM} - B_0|/B_0$ stays below $\approx 3\%$ for most of the domain; and therefore numerical diffusion is small. The orientations of the (motile) bacteria are randomly initialized. Periodic boundary conditions are enforced in all directions, for $\mathbf{u}$, C, B_M and B_{NM}.

In order to elucidate the effects of external flow on nutrient uptake and motility benefit, we solve equations 1 to 7, subject to parametric sweeps in (i) the important biological parameters at play, i.e., α_C, β_C and V_s, and, (ii) the relevant hydrodynamic parameters, i.e., drop diameter d and volume fraction of the oil phase ϕ, for drop diameters commensurate with those of an oil spill. The values of these parameters are listed in Table 1. The fluid properties $(\mu_f, \mu_g, \rho_f, \rho_g, \sigma)$ are those of Light Louisiana oil (involved in the Deepwater Horizon oil-spill) and water [36]. The size of the drops was estimated based on previous literature pertaining to droplet size distribution from sub-surface oil-spills [37, 38, 39]. The bacterial swimming speed values encompass a range from 50 to 300 μm/s. This range is expected to cover a wide variety of bacterial

species, with values $>\approx 60$ μm/s being more appropriate for marine bacteria [40]. The uptake rate constant α_C was estimated based on typical bacteria length-scales and nutrient diffusivities, as done in the first paragraph of Section 3.1. An estimate of the inverse chemotactic sensitivity, β_C, as defined by us was not available, and so we decided to cover a broad range for the values of β_C. The bacterial diffusivity was estimated from the scaling $D_b \sim V_s^2\tau/3$ [41], where V_s is the swimming speed and τ is the mean bacterial run time. For $V_s \approx 100$ μm/s, and $\tau = 1.5$ s, this yields $D_b = 5 \times 10^{-5}$ cm^2/s. But once again, numerical constraints force us to choose a larger diffusivity of $D_b = 5 \times 10^{-4}$ cm^2/s, this time for the bacteria. The reference nutrient concentration was chosen based on the values reported by Valentine *et al.* [2]. Our computational domain corresponds to a representative fluid volume ($L^3 \approx 0.15 - 9$ cm^3) consisting of mono-disperse oil drops of prescribed diameters ($d \approx 0.1 - 0.5$ cm), rising in a water column that has a patch of dissolved nutrient, as shown in Fig. 1.

3. Results and Discussion

We will first discuss some important bio-physical mechanisms at play, which will be visible in the solutions to equations 1 to 7. The initial nutrient distribution, as shown in Fig. 1(a) gets distorted once the drops rise through the fluid column. As a result, the fairly homogeneous, 'cylindrical' nutrient distribution at the vertical mid-plane gets heterogenized, leading to (i) 'breaking' or stirring of the nutrient patch into strands of varying thicknesses and concentration, and (ii) subsequent dissipation of these strands−both by the flow, and molecular diffusion−into increasingly uniform concentrations across the entire fluid domain. The chemotactic, motile bacteria forage for nutrient-rich regions, and are also transported and rotated by the flow. The non-motile organisms are simply carried by the flow, and can encounter nutrient rich regions only by chance. This fundamental difference in the ability of motile and non-motile species to access and consume nutrients is expected to yield an instantaneous chemotactic advantage to the former ($\Delta U(t) > 0$ and $R_U(t) > 1$). But this

Table 1: List of parameters. The lower and upper limits of the flow parameters correspond to $d = 0.13$ cm, and $d = 0.50$ cm, respectively. The definitions of the flow/pseudo-turbulence parameters are given in the Appendix.

Parameter (description)	**Value (units)**
Flow/physical parameters	
μ_f (viscosity of suspending fluid)	0.01 (poise)
μ_g (viscosity of dispersed phase)	0.12 (poise)
ρ_f (density of suspending fluid)	1.00 (g/cm^3)
ρ_g (density of dispersed phase)	0.85 (g/cm^3)
σ (surface tension)	40 (dyne/cm)
d (diameter of drops)	0.13 - 0.5 (cm)
$Eo = \rho_f g d^2/\sigma$ (Eötvos number)	0.41 - 6
$Ga = \rho_f^2 g d^3/\mu_f^2$ (Galileo number)	2.15×10^4 - 1.22×10^6
$\mathrm{Re}_{u'+v'+w'}$ (fluctuation Reynolds number)	0.5 - 10
ϵ_f/ρ_f (dissipation rate per unit mass)	2.7×10^{-3} - 1.2×10^{-2} (W/kg, or, m^{2}s^{-3})
$\mathrm{Re_r}$ (rise Reynolds number)	15 - 400
We (Weber number)	2.8×10^{-3} - 0.54
Bacteria/biological parameters	
V_s (swimming speed)	20 - 300 (μm/s)
α_C (nutrient uptake rate constant)	10^{-11} - 10^{-7} (cm^3/s/cell)
β_C (inverse chemotactic sensitivity)	0.4 - 4000.0 (μMcm^{-1}s)
D_b (diffusivity)	5×10^{-4} (cm^2/s)
B_0 (reference number density)	1.5×10^5 (cells/cm^3)
Nutrient	
C_0 (reference concentration)	25 (μM)
D_m (diffusivity)	5×10^{-4} (cm^2/s)
$\mathrm{Sc} = \mu_f/(\rho_f D_m)$ (Schmidt number)	2, 20
V_p/L^3 (volume fraction of nutrient patch)	2 - 8 (%)
Numerical simulation	
L (computational box length)	0.5325, 1.3564, 2.0833 (cm)
N^3 (number of grid points)	192^3
N_d (number of drops)	8, 16, 64
$h = L/N$ (smallest length scale resolved)	0.0028, 0.0071, 0.0108 (cm)

benefit diminishes because as time progresses, the heterogeneities−engendered by mechanisms described in point (i) above−are lost and the nutrient distribution relaxes to a uniform non-zero concentration. Once this relaxation occurs, there aren't any significant chemoattractant gradients left for chemotaxis to be beneficial and the chemotactic advantage ceases to exist (i.e., $\Delta U(t) \sim 0$ and $R_U(t) \sim 1$). However, nutrient consumption will continue to occur and the volume-averaged nutrient concentration will continue to decrease. Eventually, over a time scale of the order of a few hours or days (depending on the nutrient availability and consumption rate constant), the entire nutrient available will get consumed by the bacteria (both motile and non-motile) and the volume-averaged nutrient concentration will reduce to ~ 0. But this does not happen in our simulations because the time for which we run them is smaller than the time required to completely consume the entirety of the available nutrient.

The previous paragraph suggests that slower distortion of the initial nutrient field and/or faster detection of the nutrient gradients will provide maximum nutrient exposure to the motile species. Therefore, the time scale of the chemotactic response relative to that of changes in the ambient nutrient concentrations is of utmost importance. The time scale of the chemotactic response is dictated by the inverse sensitivity β_C and the swimming speed V_s, while the ambient nutrient concentration changes over a time scale governed by the flow. Another important consideration in the following discussions is the characteristic length scale associated with nutrient (and bacterial) heterogeneity l_C, i.e,

$$l_C^2 \equiv \frac{\overline{(C - C_0)^2}}{\overline{|\nabla C|^2}}, \tag{10}$$

and the volume-averaged (denoted by an over-bar) nutrient gradient $\overline{|\nabla C|}$. This latter quantity is a useful measure of the scale of the nutrient gradient being experienced by a bacterium in the flow field. Thus, any comparative analysis of the resulting dynamics is best understood by keeping in mind (i) the chemotactic and hydrodynamic time scales, and (ii) the nutrient gradient length scales. In what follows, we bring out the effect of each relevant biophysical parameter by

resorting to a comparison of the above mentioned intrinsic scales of the problem.

3.1. Influence of biological parameters, α_C, β_C and V_s

As discussed above, the nutrient strand formation is driven by fluid flow, while the localization of the bacteria in regions of high nutrient concentration is achieved by chemotaxis. This means that the biological parameters primarily govern the speed with which a nutrient 'hot-spot' is encountered. We performed simulations for a wide range of these parameters, in order to bring out their effect on the consumption process. We begin by analyzing the influence of the uptake rate constant α_C. A measure of this constant can be obtained by first calculating the uptake rate on a "per cell" basis, which is estimated from the diffusion limited uptake time scale that scales as $\tau_{diff.}^{-1} \approx aD_mB_0$, where a is the characteristic size of the bacterium [42]. For a given number density B_0, α_C then scales as $\approx (B_0\tau_{diff.})^{-1} \approx aD_m$. This gives $\alpha_C \approx O\left(10^{-8}\right)$ cm^{3}s^{-1}cell^{-1}, for $a \approx O(10)$ μm and $D_m \approx O\left(10^{-9}\right)$ m^2/s.

Fig. 3(a) shows how the instantaneous motility benefit changes with time for rate constants ranging from 1x10^{-10} cm^{3}s^{-1}cell^{-1} to 1x10^{-7} cm^{3}s^{-1}cell^{-1}. We notice a monotonic increase in the motility benefit as α_C increases. The results indicate that a faster rate of consumption translates directly to enhanced motility benefit. A physical reason for the behavior shown in Fig. 3(a) can be understood by comparing two time scales pertinent to the problem: the uptake time scale and the time scale for the persistence of nutrient gradients. A faster rate of uptake enables the motile species to profit more from staying in regions of high nutrient concentration. These regions eventually perish due to diffusion and their ephemeral nature is best exploited if the bacteria consume the nutrient rapidly enough. But we must keep in mind that higher α_C means faster consumption by the non-motile species as well. Therefore, the relative rate of consumption, i.e., the chemotactic amplification R_U stays more or less the same for each case−particularly for $\alpha_C = 10^{-10}$ and 10^{-9} cm^{3}s^{-1}cell^{-1}−as seen in Fig. 4(a). In other words, any advantage offered to the motile species by an increase in α_C is offered equally to the non-motile species, resulting in no

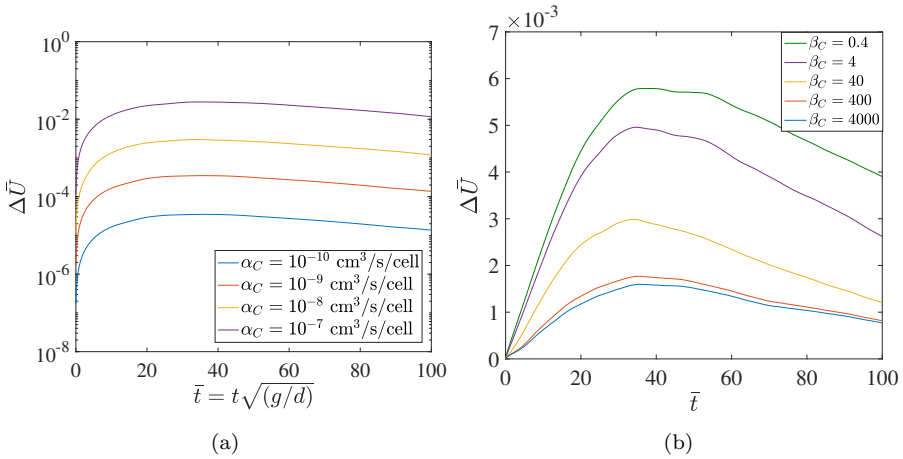

Figure 3: (Color online) (a) Time evolution of the dimensionless motility benefit for different uptake rate constants (α_C). $\beta_C = 40.0$ μMcm^{-1}s. (b) Time evolution of the dimensionless motility benefit for different inverse chemotactic sensitivities (β_C); the units of β_C are μMcm^{-1}s. $\alpha_C = 1\text{x}10^{-8}$ cm^{3}s^{-1}cell^{-1}. The other parameters are: $d = 1.32$ mm; $\phi \approx 11\%$; V_s=100 μms^{-1}; $D_m = D_b = 5\text{x}10^{-4}$ cm^2/s; $C_0 = 25$ μM; $B_0 = 1.5\text{x}10^5$ cells/cm^3; $Eo = 0.40$; $Ga = 2\text{x}10^4$.

relative benefit for the former. Our calculations show that, for the parameters of Fig. 3, the motile bacteria consume the nutrient $\approx 5\%$ ($\Delta U/\dot{C}_{NM} \approx 0.05$) faster than the non-motile ones, irrespective of the value of α_C.

The next biological parameter we consider is the inverse chemotactic sensitivity β_C (see equation 4). This parameter is only relevant for motile bacteria. It is a measure of the time taken by a chemotactic bacterium to reorient towards the direction ∇C, i.e., in the direction of increasing concentration of the chemoeffector C. Lower values of β_C indicate one of the following two scenarios: (i) for a fixed $|\nabla C|$, the bacterium rotates more rapidly to attain a swimming direction along ∇C, or (ii) the bacterium is able to sense subtler spatial gradients in its vicinity, and reorient accordingly. Fig. 3(b) shows a series of curves wherein the value of the dimensionless motility benefit, $\Delta\bar{U}(t)$, increases progressively, as β_C is reduced from 4000.0 μMcm^{-1}s to 0.4 μMcm^{-1}s. This is an implication of the balance between the two reorientation effects in equation 4: rotation due

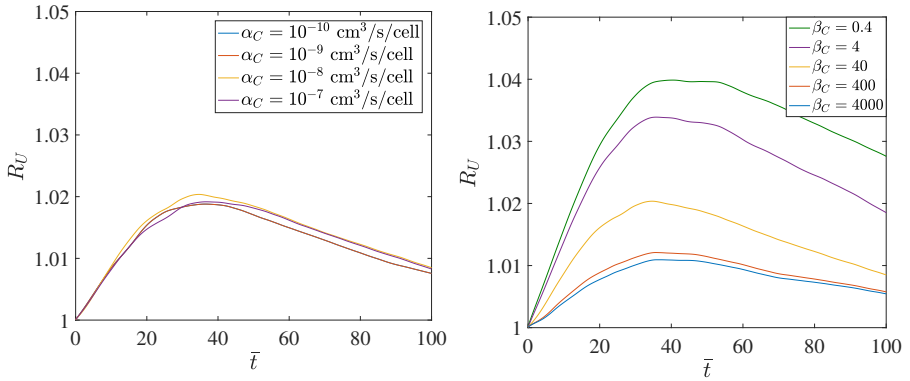

(a) (b)

Figure 4: (Color online) (a) Time evolution of the chemotactic amplification factor for different uptake rate constants (α_C). $\beta_C = 40.0$ μMcm^{-1}s. Clearly, a change in α_C does not affect the relative consumption rates significantly, because it proportionately enhances the values of $\dot{C}_M$ and $\dot{C}_{NM}$. (b) Time evolution of the chemotactic amplification factor for different inverse chemotactic sensitivities (β_C); the units of β_C are μMcm^{-1}s. $\alpha_C = 1\text{x}10^{-8}$ cm^{3}s^{-1}cell^{-1}. The other parameters are: $d = 1.32$ mm; $\phi \approx 11\%$; V_s=100 μms^{-1}; $D_m = D_b = 5\text{x}10^{-4}$ cm^2/s; $C_0 = 25$ μM; $B_0 = 1.5\text{x}10^5$ cells/cm^3; $Eo = 0.40$; $Ga = 2\text{x}10^4$.

to the ambient vorticity ($\boldsymbol{\omega} \times \mathbf{p}$) vs. rotation as a response to local gradients in C $\left(\beta_C^{-1} \left(\mathbf{I} - \mathbf{pp}\right) \cdot \nabla C\right)$. The rotation due to ambient vorticity dominates for large values of β_C, and although bacteria always tend to rotate towards the direction of increasing nutrient concentration, they are unable to do so quickly enough. This reveals a second balance of time scales inherent in our problem: the competition between $|\omega|^{-1}$ (the time scale for reorientation by flow) and $\frac{\beta_C}{|\nabla C|}$ (a chemotactic reorientation time scale). As long as $\frac{\beta_C}{|\nabla C|} > |\omega|^{-1}$, the reorientation will predominantly be due to the local rotation rate of the fluid. In this case, the possibility of chemotaxis being beneficial is contingent on the proximity of motile bacteria to regions of high concentration gradients (large values of $|\nabla C|$), because low values of $|\nabla C|$ prove insufficient to overcome the tendency of hydrodynamics-induced reorientation. Scaling analysis reveals that in order for chemotactic reorientation to be effective, β_C must be $\leq \frac{|\nabla C|}{(u_c/l_{ref})}$; which gives—for parameters used in Fig. 3(b)—$\beta_C \leq O(10)$ μMcm^{-1}s.

Fig. 3(b) shows that the increase of motility benefit $\Delta\bar{U}(t)$ is not always commensurate with the increase in β_C^{-1}, particularly when β_C is very large (least sensitive chemotaxis) or small (most sensitive chemotaxis). The rate of increase in max. $\left\{\Delta\bar{U}\right\}$ —with respect to β_C—becomes smaller when β_C reduces. This suggests an upper limit to the chemotactic advantage that can be offered by enhanced sensitivity to gradients in nutrient concentration. This is seen in the reduced difference in the motility benefit curves for $\beta_C = 4.0$ μMcm^{-1}s to 0.4 μMcm^{-1}s, and quantified in Fig. 5. It is also apparent that the value of $\Delta\bar{U}(t)$ for $\beta_C = 4000.0$ μMcm^{-1}s to 400.0 μMcm^{-1}s is not substantial. This observation corresponds to a regime where chemotaxis is not as significant in re-orienting the bacteria as hydrodynamics. Thus, we conclude that $\beta_C \geq O(100)$ μMcm^{-1}s represents negligible effect of ∇C on the bacteria's orientation, while $\beta_C \leq O(10)$ μMcm^{-1}s represents almost instantaneous reorientations to ambient ∇C. A true coupling of the chemotactic and hydrodynamic reorientation effects takes place only for the intermediate values of β_C ($O(10)$ μMcm^{-1}s $\leq \beta_C \leq O(100)$ μMcm^{-1}s). Fig. 4(b) shows that higher chemotactic sensitivity (low β_C) enhances the total uptake by 4% for $V_s = 100$ μm/s. This factor

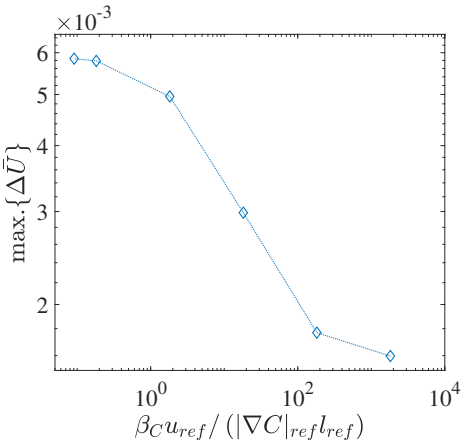

Figure 5: (Color online) Variation of the maximum value of the dimensionless instantaneous motility benefit, max.$\{\Delta\bar{U}\}$, with β_C scaled by $\left(|\nabla C|_{ref} l_{ref}/u_{ref}\right)$. The motility benefit increases with the chemotactic sensitivity (inverse of β_C), but not indefinitely; a saturation occurs for $\beta_C < 0.4\mu\text{Mcm}^{-1}\text{s}$.

increases for higher swimming speeds, which is discussed next.

The swimming speed is another biological factor that allows marine bacteria to exploit gradients in nutrient concentration. Since diffusion tends to smoothen all gradients, it is imperative that the bacteria swim to nutrient-rich regions as fast as possible. This balance between the diffusion and the chemotactic time scales is one of the most important factors in determining the extent to which motility can be beneficial in marine environments [11]. Fig. 6(a) brings out the effect of swimming speeds on the motility benefit, with speeds ranging from 50 to 300 μm/s; a range of values that is typical for marine bacteria. The first feature we observe is that increasing V_s has a fairly monotonous effect on the consumption characteristics: faster bacteria profit considerably. This is a direct consequence of the chemotactic time scale being progressively shorter than the diffusion time scale, as V_s is increased. This means that under identical conditions, a faster bacterium will be able to travel deeper into the nutrient-rich regions as compared to a slower bacterium. Just like β_C, V_s only affects the performance of the motile species, and so higher swimming speeds also lead to an increase in the relative consumption, as shown in Fig. 6(b). An interesting

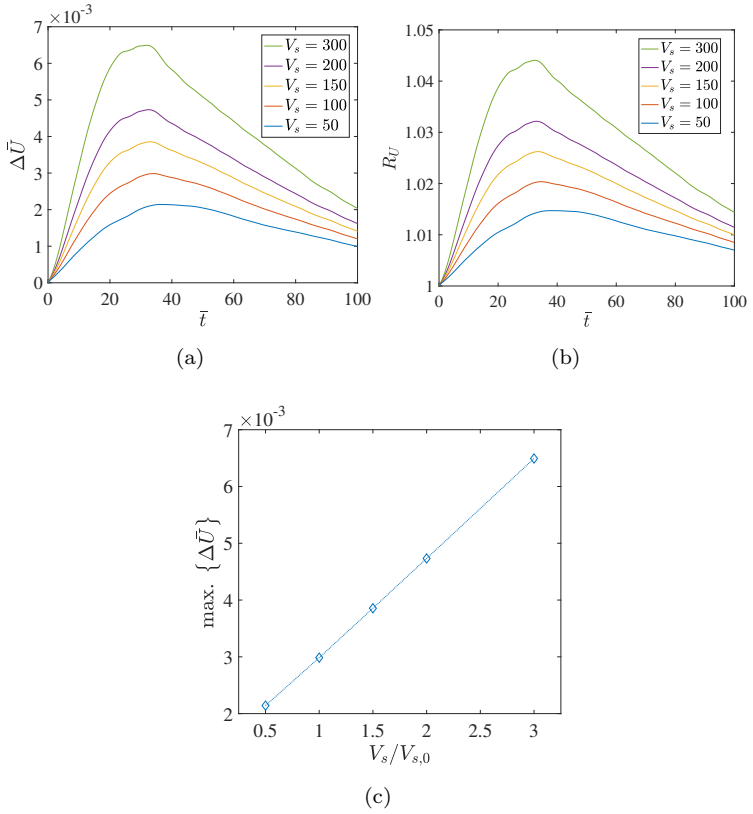

Figure 6: (Color online) (a) Time evolution of the dimensionless motility benefit for different swimming speeds. (b) Time evolution of the chemotactic amplification for different swimming speeds; the units of V_s are μm/s. (c) The maximum motility benefit scales linearly with the swimming speed ($V_{s,0} = 100$ μm/s). The other parameters are: $d = 1.32$ mm; $\phi \approx 11\%$; $\alpha_C = 1\text{x}10^{-8}$ cm^{3}s^{-1}cell^{-1}; $\beta_C = 40.0$ μMcm^{-1}s; $D_m = D_b = 5\text{x}10^{-4}$ cm^2/s; $C_0 = 25$ μM; $B_0 = 1.5\text{x}10^5$ cells/cm^3; $Eo = 0.40$; $Ga = 2\text{x}10^4$.

observation is the dependence of the maximum motility benefit on the normalized swimming speed $V_s/V_{s,0}$; which is linear for a wide range of swimming speeds, as shown in Fig. 6(c). This is an important result because it allows us to estimate the motility benefit at different swimming speeds of the bacterium under more varied conditions set by the other parameters involved. One can estimate the maximum possible enhancement in the consumption rate by noting two things: (i) for the highest chemotactic sensitivity ($\beta_C = 0.4\ \mu\mathrm{Mcm}^{-1}s$), the consumption is enhanced by $\approx 4\%$, and, (ii) the maximum motility benefit scales linearly with the swimming speed V_s. One subtle aspect of higher swimming speeds leading to enhanced consumption is the assumption that the span of nutrient-rich regions is wide enough to ensure that they are not simply bypassed by the faster bacteria. There is a trade-off between reaching nutrient-rich regions faster and staying there for as long as possible [11]. Based on the results of our simulations, the spatial extent of nutrient-rich regions is wide enough for increased V_s to pose significant benefits.

To conclude this Section, we stress on the nature of dependence of $\Delta\bar{U}$ and R_U on each of the biological parameters studied. We saw that a the change in α_C only affects $\Delta\bar{U}$ and not R_U, because increasing α_C increases the consumption rate by *both* motile and non-motile bacteria. But an increase in β_C and V_s affects *only* the consumption by motile bacteria, and thus results in significant changes in both $\Delta\bar{U}$ and R_U. In case of V_s, the chemotactic advantage is derived from faster gradient climbing, which enables the fast bacteria to seek out proportionately higher nutrient concentrations and increase the uptake rate. Therefore, the maximum motility benefit achieved increases linearly with V_s. The variation of $\Delta\bar{U}$ with β_C is more complex and the response of Fig. 3(b) is due to the continuously evolving nature of both ∇C and $|\boldsymbol{\omega}|$, and their interaction via equation 4. The apparent saturation in instantaneous $\Delta\bar{U}(\bar{t})$ for low values of β_C is due to purely chemotactic reorientations; while negligible $\Delta\bar{U}(\bar{t})$ for high values of β_C can be attributed to purely hydrodynamic reorientations.

3.2. Influence of physical parameters: drop diameter and volume fraction

Biological parameters like the ones discussed above are only one set of properties that can influence the nutrient consumption by motile and non-motile bacteria. Another set of properties comes from the hydrodynamic aspects of oil spill, namely the diameter of the rising drops and their volume fraction. These properties change the background flow field and in this way, fundamentally alter the process of chemotaxis. While there was very little qualitative change in the evolution of the nutrient field in the DNS of the previous set of results, we cannot say the same when the background hydrodynamics−the major cause of nutrient redistribution−itself is different. The size and volume fraction of the rising oil drops can drastically change the length scales of the nutrient strands and the time scales of their transport through the domain. It will also directly affect the transport of the bacteria (see equations 3 and 4), thus providing us with a wide array of bio-physical effects to investigate. We study these effects systematically by: (a) first varying the diameter of the drops but keeping the volume fraction constant; and then (b) varying the volume fraction of the oil but keeping the drop diameters constant, in order to facilitate comparisons between the various cases considered.

Fig. 7(a) shows evolution of the amplification factor $R_U(t)$ as a function of the diameter of the oil drops. It is to be noted that in all of the cases described, the size of our representative system (i.e., the computational domain) is adjusted such that the volume fraction of the oil phase remains the same. We note that dispersants are often used in oil spill remediation efforts to help break the oil into smaller droplets by reducing the interfacial tension between water and oil. The reduced drop diameters (due to break up) increase the effective surface area of the oil phase, making it easier for the biodegrading agents to break down the heavier (insoluble) HCs released in the oil spill. Here, we show that this also has an indirect effect on the degradation of the soluble HCs, as the flow field around the rising drops depends heavily on the drop diameter, via the Eötvos and the Galileo numbers. The drop diameters for a surfactant-laden oil phase are typically ≈ 1 mm or smaller, and those for a pure oil phase

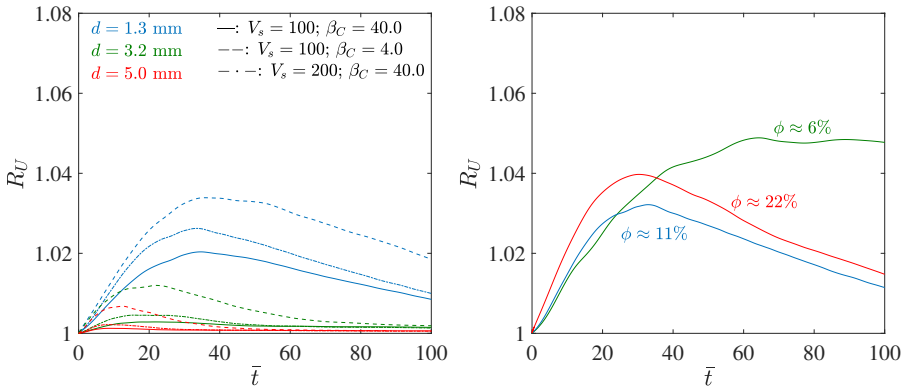

Figure 7: (Color online) (a) Time evolution of the chemotactic amplification factor, for different drop diameters, but same volume fraction in all cases: $\phi \approx 11\%$. The units of V_s are μm/s, and of β_C are $\mu\text{Mcm}^{-1}\text{s}$. (b) Time evolution of the chemotactic amplification factor, for different volume fractions, but same drop diameters in all cases. $Eo = 0.40$; $Ga = 2\text{x}10^4$. $d \approx 1$ mm. The other parameters are: $\alpha_C = 1\text{x}10^{-8}$ $\text{cm}^3\text{s}^{-1}\text{cell}^{-1}$; $D_m = D_b = 5\text{x}10^{-4}$ cm^2/s; $C_0 = 25$ μM; $B_0 = 1.5\text{x}10^5$ cells/cm^3. We would like to emphasize that the motility benefit, $\Delta\bar{U}$, follows an identical trend as the amplification factor, R_U, and therefore is not shown here ($\max\left\{\Delta\bar{U}\right\} = 0.006$).

emanating from a leak are $\approx$ 5 mm or larger [37, 38, 39]. In this Section, we investigate the dependence of the amplification factor on d, for three drop diameters, spanning across a range that includes the aforementioned sizes. We see a marked difference in the values of $R_U(\bar{t})$ for the three cases, as shown in Fig. 7(a). The amplification is seen to be the highest for the smallest drop diameters. In fact, for the largest diameters (the red lines in Fig. 7(a)) motility doesn't lead to any significant advantage whatsoever, irrespective of changes in the two most important biological parameters$-V_s$ and β_C-governing the sensitivity of motile bacteria to ambient gradients. The advantage offered by high swimming speeds and/or high chemotactic sensitivity seems to get enhanced as the diameter of the oil drops is reduced. The first effect (increased sensitivity to V_s with lower d) is a direct consequence of the length scales traversed by the motile bacteria to reach the high-concentration regions, which scale as l_c (see equation 10), and are much

shorter for smaller drop diameters. In fact, it is seen that $l_C \approx O(1)$ mm for $d = 1$ mm, and $l_C \approx O(100)$ mm for $d = 5$ mm (see Fig. 12 in Appendix). The second effect (increased sensitivity to β_C with lower d) is also directly attributed to a change in the drop diameters; with smaller drops engendering stronger gradients, and faster reorientations. When the characteristic length scale of the problem decreases, it leads to a proportional increment in the magnitude of concentration gradients, making chemotaxis more effective. Thus, even though the spatial extent of heterogeneities increases with increasing drop diameters, the gradients within these heterogeneities are not strong enough to provide sufficient advantage to motile bacteria. We note that larger drop diameters also mean reduced values of the characteristic vorticity ($|\boldsymbol{\omega}| \approx \sqrt{g/d}$), but this just means that bacteria do not change their swimming directions fast enough even due to rotation by the flow. In such a scenario, the bacteria do not deviate much from their initial swimming direction, and it can be said that their encounter with nutrient-rich regions depends heavily on them simply straying into regions with high enough values of C, or $|\nabla C|$. In light of this discussion, the results presented in Fig. 7(a) suggest a potential benefit that may be incurred by motile bacteria if dispersants are used during an oil spill.

Finally, we discuss what happens if the volume fraction ϕ of oil in the oil-water system changes, but the diameter of the drops remains the same. This parameter is a reasonable metric to quantify the intensity of any leak, with higher volume fractions representative of regions of intense dispersive activity by the rising, insoluble HCs. In the DNS, we simply change the number of drops occupying the computational domain to change the volume fraction of the system. We analyze small drop diameters ($d \approx 1$ mm) so as to characterize chemotactic advantages that are significant. Our studies indicate a non-trivial temporal evolution of the chemotactic amplification as a function of the volume fraction. There are significant differences, both in the maximum amplification achieved, the time scale at which said maximum is reached, and the rate of the eventual decay in $R_U(t)$. The maximum value of R_U is higher for $\phi \approx 6\%$ and $\phi \approx 22\%$, than it is for $\phi \approx 11\%$. This increase in the maximum value of R_U

either side of $\phi \approx 11\%$ can be explained by examining how the nutrient patch deforms in the two cases. The pseudo-turbulent dissipation rate increases as the volume fraction of the system increases [7]. In our study, the values of the steady state dissipation rates per unit mass (in the suspending fluid) for $\phi \approx 22\%, 11\%$ and 6% are 9.3×10^{-3} W/kg, 4.3×10^{-3} W/kg and 2.7×10^{-3} W/kg, respectively. Thus, the nutrient dispersion−which increases monotonically with the dissipation rate in the fluid [11]−is fastest for $\phi \approx 22\%$ and slowest for $\phi \approx 6\%$. This results in more intense stirring of the nutrient in the former case, leading to a relatively higher initial availability of the nutrient, and thus an earlier peak in R_U. But high dissipation rate also means faster mixing. The strong gradients that form disappear equally quickly and therefore the chemotactic advantage isn't sustained for long. The behavior for $\phi \approx 6\%$ is exactly opposite, wherein the initial distribution is not 'broken' quickly enough. This can be explained by considering the anisotropy in the fluid velocity fluctuations, or equivalently, the same for the drop velocity fluctuations: $\overline{\mathrm{Re}}_{u'}/\overline{\mathrm{Re}}_{v'+w'}$ [6, 7]. This ratio is a measure of the dispersion of the nutrient in the rise-direction, as compared to the dispersion transverse to the rise-direction. Its values for $\phi \approx 6\%, 11\%$, and 22%, are 3.3541, 1.4248 and 1.3403, respectively. Clearly, for the lowest volume fraction, there isn't appreciable transverse dispersion due to pseudo-turbulence. As a result, the nutrient is not distributed over an appreciable region of the domain early on in the simulations. But this also means that it takes greater time for the nutrient to diffuse away to a uniform background concentration. Therefore, for $\phi \approx 6\%$, the chemotactic species get ample time to populate the nutrient-rich regions, and so a maximum in R_U is reached, but much later than that for $\phi \approx 22\%$. The motile bacteria are afforded more nutrient-rich regions, and importantly, for longer times, if the fluid flow is driven by a lower volume fraction of drops. This prolongation of the chemotactic advantage−and a very gradual decay−is readily seen in Fig. 7(b). For $\phi \approx 11\%$, the two effects−initial nutrient stirring and eventual homogenization−balance each other and neither one is dominant enough. Thus, the amplification for $\phi \approx 11\%$ is not stronger than $\phi \approx 6\%$ because of relatively faster homogenization of the nutrient, and is

not stronger than $\phi \approx 22\%$ because of relatively slower initial dispersion of the cylindrical nutrient patch. Finally, we emphasize that for the range of parameters considered in Fig. 7(b), the average rise Reynolds number of the system does not vary much with the volume fraction ($\mathrm{Re_r} \approx 15 - 35$); leading us to believe that it is solely the aforementioned chemotactic interactions of the bacteria with the nutrient field−and not the specific bacterium-flow interactions−that result in the varied behavior exhibited in this Section.

4. Chemotactic amplification vis-à-vis nutrient availability

We have seen how different bio-physical parameters shape the evolution of the motility benefit $\Delta\bar{U}(\bar{t})$ and the chemotactic amplification $R_U(\bar{t})$, in pseudo-turbulent flows generated by a swarm of rising drops. The motility benefit only quantifies the difference between the consumption rates of motile and non-motile bacteria, but does not fully specify the advantages of motility, e.g., even though $\Delta\bar{U}(\bar{t})$ increases with α_C, $R_U(\bar{t})$ remains unchanged, indicating that for the parameter values considered, faster consumption doesn't necessarily help the motile bacteria exclusively. On the other hand, whenever motile bacteria are provided an exclusive advantage (i.e., motility results in higher relative rates of consumption), the nature of the variation of $R_U(\bar{t})$ and $\Delta\bar{U}(\bar{t})$ is almost identical. Therefore, the importance of defining a second metric to quantify chemotactic advantage doesn't become immediately obvious. But whenever the nutrient availability is low, the value of $\Delta\bar{U}(t)$ is bound to be smaller than the cases where the nutrient availability is high [27]. In such cases it is more instructive to assess the chemotactic advantage in terms of the chemotactic amplification factor.

Fig. 8 highlights the importance of measuring the quantity R_U. It can be seen that the absolute motility benefit $\Delta\bar{U}$ is higher when the initial nutrient volume (V_p) is higher, but maximum amplification occurs for the case in which V_p is *lower*. This shows how motile bacteria are expected to profit most from situations where nutrient availability is sparse. It is also seen that the motility

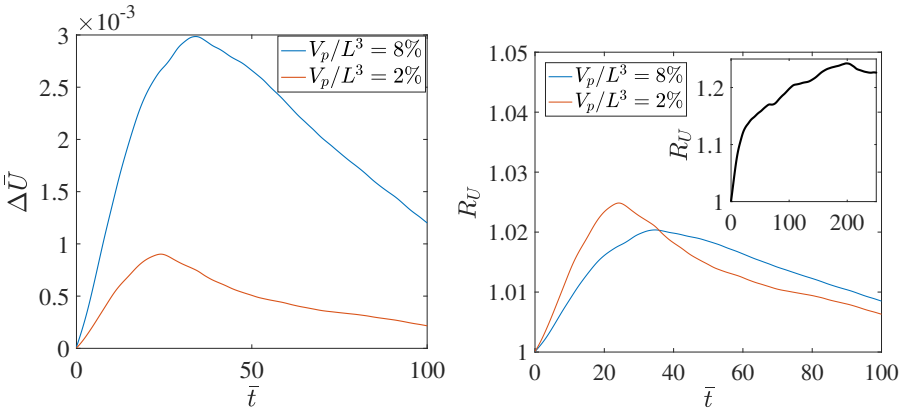

Figure 8: (Color online) (a) Time evolution of the dimensionless motility benefit, for different nutrient availabilities (volume of the nutrient patch V_p, normalized by the volume of the computational domain L^3). (b) Time evolution of the chemotactic amplification factor, for the same nutrient availabilities as in part (a). The inset shows the case of maximum $R_U \approx 24\%$ obtained in our study (for $d \approx 1$ mm, $\phi \approx 6\%$, $V_s = 300$ μm/s, $\beta_C = 0.4$ μMcm^{-1}s, and $V_p/L^3 = 2\%$). Note the significant increase in the time taken to reach a maximum in R_U, and as a consequence, an almost 4-fold prolongation of the motility benefit as compared to the baseline simulations. While the maximum is reached somewhere around $\bar{t} \approx 50$ in the baseline simulations, it takes $\bar{t} \approx 200$ to observe a maximum for the inset. The other parameters for the main figures (a) and (b) are: $Eo = 0.40$; $Ga = 2\text{x}10^4$; $d \approx 1$ mm; $\phi = 6\%$; $\alpha_C = 1\text{x}10^{-8}$ cm^{3}s^{-1}cell^{-1}; $D_m = D_b = 5\text{x}10^{-4}$ cm^2/s; $C_0 = 25$ μM; $B_0 = 1.5\text{x}10^5$ cells/cm^3.

benefit and the amplification factor decay to zero and to unity respectively, much faster for lower values of V_p. This is because of the smaller nutrient patch being mixed up faster. Therefore, even though low nutrient availabilities favor consumption by motile species, this advantage doesn't last for long.

In our studies, the chemotactic amplification varies from being negligible ($< 1\%$) for the larger values of d and ϕ, to $\approx 24\%$ for systems where $d \approx 1$ mm, $\phi \approx 6\%$, swimming speeds are particularly high, and nutrient availability $V_p/L^3 = 2\%$, as seen in the inset in Fig. 8(b). An important observation is that under suitable conditions, chemotaxis leads to significant prolongation of the motility benefit: up to 4 times longer than the time durations for the baseline simulations. The amplification factor is expected to increase even more if the availability of nutrient is limited to $\approx 1\%$ of the computational domain by volume. We emphasize that due to our choice of a much higher nutrient (and bacteria) diffusivity than usual, the values of R_U and $\Delta\bar{U}$ are under-predicted for the results discussed thus far. An examination of the chemotactic advantage for lower diffusivities, along with $V_p/L^3 = 1\%$, yields an upper limit of chemotactic amplification to be $\approx 45\%$ (see Fig. 10 in the Appendix, and the accompanying discussion). This particular scenario is quintessential for any chemotactic species to profit heavily, and represents the case where $\Delta\bar{U}(t)$ is extremely small, yet the nutrient has been consumed almost exclusively by the motile bacteria.

5. Conclusion

In this paper, we quantified the chemotaxis driven consumption of a dissolved chemoeffector in the presence of a rising swarm of oil drops, and unraveled the role of motility on the consumption dynamics. The pseudo-turbulence induced by the rising drops causes significant dispersion of the nutrient patches in the water column. The motile bacteria−capable of chemotactic foraging−benefit from local gradients in nutrient concentration to reach nutrient-rich regions. They thus gain an advantage which is unavailable to their non-motile, non-

chemotactic counterparts, that rely solely on the ambient flow to carry them towards any nutrient hot-spots. The maximum motility benefit is seen to saturate with enhanced chemotactic sensitivity, and is seen to increase linearly with the swimming speed. Lower volume fractions of the dispersed (oil) phase prove beneficial to the motile bacteria, owing to less vigorous mixing−and consequently greater availability−of nutrient-rich regions. The motility benefit for low volume fractions is seen to extend to much longer times. On the other hand, higher volume fractions also prove advantageous, because they increase the initial availability of the nutrient to the motile bacteria by vigorously dispersing the nutrient patch. The most important effect of the hydrodynamic factors, however, is the significant difference between the instantaneous values of motility benefit, for larger oil drops versus those for smaller oil drops (that could result due to addition of dispersant). This difference stems from the relatively weaker nutrient gradients formed in the former case, which do not prompt sufficiently strong chemotaxis, thus reducing the disparity between the behaviors of motile and non-motile species. In terms of relative rates of consumption, we find that motility can provide an advantage ranging from a $O(1)\%$ to $\approx 24\%$ faster consumption of the available nutrient, depending on the parameters detailed above and the spatial scale of a nutrient patch. We estimate that lower nutrient diffusivities lead to even more advantageous conditions for chemotactic bacteria, and an amplification of $\approx 45\%$ can be achieved if the chemotaxis is strong enough, the initial nutrient availability is restricted to 1% of the domain, and the fluid flow is driven by a low ($\approx 6\%$) volume fraction of oil drops. Our study provides useful insights, and scope for experimentation, into the role of droplet size on the microbial biodegradation of dissolved HCs in marine environments.

Appendix

We provide the definitions of the various pseudo-turbulence parameters given in Table 1. These definitions are borrowed from the papers by Bunner and Tryggvason [6, 7]. The volume-averaged velocities of the dispersed phase (oil drops)

are given by $\mathbf{V}_g = (U_g, V_g, W_g)$, and those of the suspending fluid (water) are given by $\mathbf{V}_f = (U_f, V_f, W_f)$. The slip velocity between the two phases is defined as, $\mathbf{V}_r = \mathbf{V}_g - \mathbf{V}_f$, and the rise Reynolds number as, $\mathrm{Re_r} = \rho_f \left|\mathbf{V}_r\right| d/\mu_f$. The velocity of the center of mass of the l^{th} drop, $\mathbf{V}_g^{(l)}$, is obtained by differentiating its position, $\mathbf{r}_g^{(l)}$, with respect to time:

$$\mathbf{V}_g^{(l)}(t) = \frac{d\mathbf{r}_g^{(l)}}{dt}, \tag{11}$$

and the instantaneous volume-averaged velocity of the dispersed phase, $\mathbf{V}_g(t)$, is then obtained by averaging $\mathbf{V}_g^{(l)}$ over all the drops:

$$\mathbf{V}_g(t) = \frac{1}{N_d}\sum_{l=1}^{N_d} \mathbf{V}_g^{(l)}(t); \tag{12}$$

finally, $\mathbf{V}_g$ is obtained by the following time-averaging:

$$\mathbf{V}_g = \frac{1}{T}\int_T \mathbf{V}_g(t)\, dt, \tag{13}$$

and the Weber number is defined as, $\mathrm{We} = \rho_f U_g^2 d/\sigma$. The fluctuation Reynolds number $\mathrm{Re}_{u'+v'+w'}$ is defined based on the fluctuation velocities of the dispersed phase, which we define next. The instantaneous fluctuation velocities are defined as:

$$V'_{g_i}(t) = \sqrt{\frac{1}{N_d}\sum_{l=1}^{N_d}\left(V_{g_i}^{(l)}(t) - V_{g_i}(t)\right)^2}, \tag{14}$$

where, $i = 1, 2, 3$ refers to the velocities along the x, y, z directions, respectively. The fluctuation Reynolds number is then given by:

$$\mathrm{Re}_{u'+v'+w'} = \frac{\rho_g\left(U'^2 + V'^2 + W'^2\right)^{1/2} d}{\mu_g}, \tag{15}$$

and the *mean* fluctuation Reynolds number by:

$$\overline{\mathrm{Re}}_{u'+v'+w'} = \sqrt{\frac{1}{T}\int_{t=0}^{T} \mathrm{Re}^2_{u'+v'+w'}(t)\, dt}, \tag{16}$$

where $U' = V'_{g_1}, V' = V'_{g_2}, W' = V'_{g_3}$, and T is the time for which the simulations are run. The pseudo-turbulent dissipation rate per unit volume of

the suspending fluid (water), ϵ_f, is given by:

$$\begin{aligned} \varepsilon_{fij} &= \tfrac{1}{2\Omega_f} \int_{\Omega_f} \mu \Big(\tfrac{\partial u_i}{\partial x_j} + \tfrac{\partial u_j}{\partial x_i} \Big)^2 dV, \\ \varepsilon_f &= \sum \varepsilon_{fij}, \end{aligned} \tag{17}$$

where Ω_f is the total volume of the suspending liquid. The dissipation rate on a per unit mass basis is given by ϵ_f/ρ_f.

Fig. 9 shows the time evolution of the dimensionless motility benefit and the chemotactic amplification factor, for two cases: one with $D_R \neq 0$ (dashed lines) and another with $D_R = 0$ (solid lines). All our results have been generated using the latter assumption, and it is clear from the negligible difference between the two cases in Fig. 9 that our assumption is justified for the present scenario.

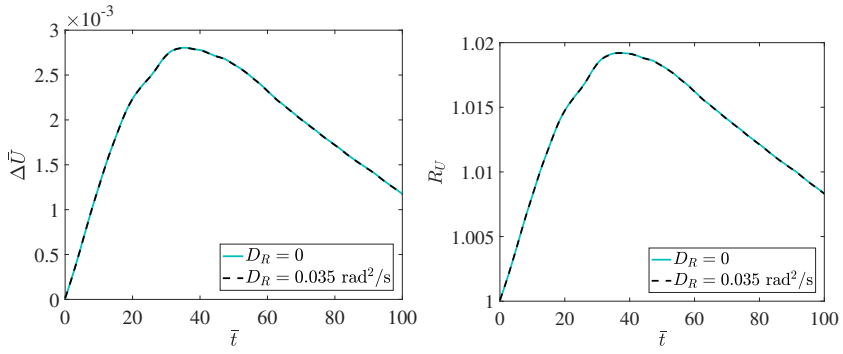

(a) (b)

Figure 9: The effect of rotary diffusivity (in the equation governing the orientation of the bacteria, i.e., equation 4) on the instantaneous motility benefit $\Delta\bar{U}$ and the chemotactic amplification R_U. We conclude that as long as there exists a background flow that is strong enough, the rotary diffusivity can be safely neglected. The value of D_R is borrowed from a reference calculating the same for the marine bacterium *V. alginolyticus* [43].

Fig. 10 details the influence of nutrient diffusivity, D_m, on the chemotactic amplification. A comparison between the plots for Sc = 2, 20 and 666 reveals trends that can be used to estimate the consumption dynamics for more realistic nutrient diffusivities ($10^{-5} - 10^{-9}$ cm^2/s). Note that for Sc = 666, $D_m = 1.5 \times 10^{-5}$ cm^2/s; a value that lies on the upper limit of realistic nutrient diffusivities and is indicative of the diffusivity of methane in water [44].

We also stress that the DNS for Sc = 666 is not fully resolved: there is a 5% error in the values of volume-averaged consumption rates, and a 15% error in the values of RU, between the highest and the second highest grid resolutions used. Nevertheless, the results of Fig. 10, for Sc = 666, do provide an approximation of the chemotactic advantage for more realistic diffusivity values. The first observation is that R_U decays faster as nutrient diffusivity increases (Sc decreases); though this effect is most pronounced for the smallest Schmidt number. Secondly, R_U is much less sensitive to the swimming speed for higher nutrient diffusivities. Both these behaviors occur because the time scale for the smearing away of nutrient gradients is faster if the nutrient's diffusivity is large, and thus nutrient hot-spots do not persist long enough to yield greater motility benefit and chemotactic amplification for a given increase in the swimming speed. One can thus say that for nutrient diffusivities lower than that considered in this paper (i.e., for $D_m < 5 \times 10^{-4}$ cm^2/s, Sc > 20), the chemotactic advantage will extend for longer times and the biological parameters−swimming speed and chemotactic sensitivity−will more significantly affect the magnitude of the motility benefit and the chemotactic amplification. See for example, the inset in Fig. 10, wherein a 45% amplification in the overall nutrient consumption is observed, for fairly strong chemotaxis ($V_s = 300$ μm/s, $\beta_C = 4 \times 10^{-7}$ Mcm^{-1}s), low nutrient availability ($V_p/L^3 = 1\%$), and low volume fraction of oil drops ($\phi \approx 6\%$). In this way, we demonstrate that the results of this study are indeed a conservative estimate of the actual chemotactic advantage that can be derived by marine bacteria in their search for nutrients.

The effect of the shape of the initial nutrient patch on the chemotactic advantage is shown in Fig. 11. The initial behavior is identical irrespective of the shape of the nutrient patch and so is the behavior after the attainment of the maximum; but the maximum value of the motility benefit and chemotactic amplification is different in the three cases considered. We find that if the initial shape is a cylinder with axis perpendicular to the direction of gravity−i.e., along the y axis−then the chemotactic advantage is reduced significantly after some time. This behavior can be attributed to the fact that the nutrient patch

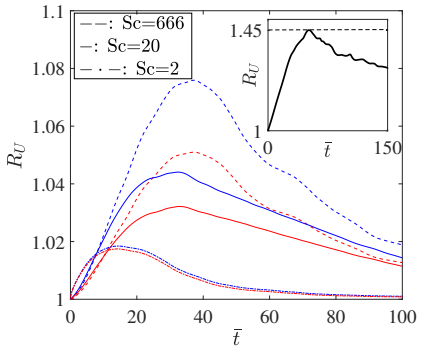

Figure 10: The effect of nutrient diffusivity on the chemotactic amplification R_U. The variation is shown as a function of the swimming speed V_s (200 (red) and 300 μm/s (blue)). As evident from Fig. 6, the higher R_U values correspond to the higher swimming speeds. Inset: A significant chemotactic amplification of 45% is observed for $D_m = 1.5 \times 10^{-5}$ cm^2/s (Sc = 666), if the nutrient availability is lowered to $V_p/L^3 = 1\%$. The values of the hydrodynamic parameters for the inset are the same as those for $\phi \approx 6\%$ in Fig. 7, and the values of the biological parameters are given in the main text.

perpendicular to the drops' average rise direction gets distorted and homogenized much faster than one which is along the direction in which the drops rise. The same is true for the spherical nutrient patch, although the difference in the maximum is not as significant. A key point is that although there exists a quantitative difference, the qualitative evolution is very similar in all three cases. This leads us to believe that the nature of variation of the chemotactic advantage, with respect different biophysical parameters, should be similar for the three different patch-shapes.

Finally, the length scales used to describe the results of Fig. 7(a) in Section 3.2 are quantified in Fig. 12. We note a direct correlation between low values of $\bar{l}_C$ (or, high values of $|\overline{\nabla C}|$) and high values of $\Delta\bar{U}$.

Conflicts of interest

There are no conflicts to declare.

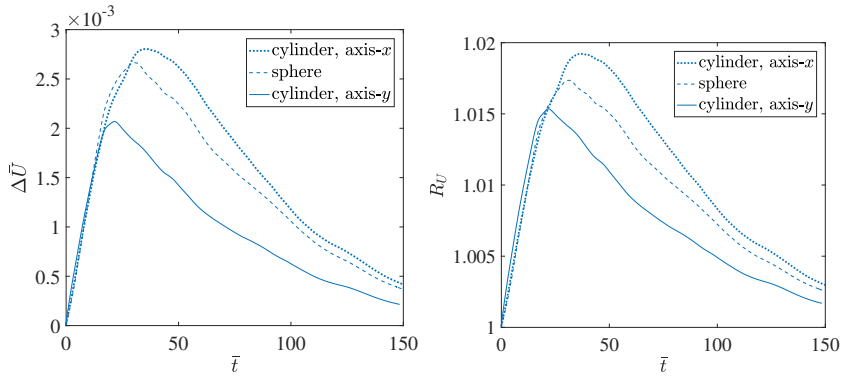

Figure 11: Time evolution of the (a) instantaneous motility benefit $\Delta\bar{U}$, and, (b) amplification factor R_U, as a function of the initial shape of the chemoattractant patch. The spherical patch has the same volume as the cylindrical; 'axis' refers to the direction along which the axis of the cylindrical patch is oriented. The other parameters are: $\alpha_C = 1\text{x}10^{-8}$ cm^{3}s^{-1}cell^{-1}; $\beta_C = 40.0$ μMcm^{-1}s; $V_s = 100$ μm/s; $D_m = D_b = 5\text{x}10^{-4}$ cm^2/s; $C_0 = 25$ μM; $B_0 = 1.5\text{x}10^5$ cells/cm^3.

Acknowledgement

This research was made possible by grants from the Gulf of Mexico Research Initiative and the NSF, CBET-1604423, CBET-1705371.

References

[1] I. M. Head, D. M. Jones, W. F. M. Röling, Marine microorganisms make a meal of oil, Nature Reviews Microbiology 4 (3) (2006) 173–182. doi:10.1038/nrmicro1348.

[2] D. L. Valentine, J. D. Kessler, M. C. Redmond, S. D. Mendes, M. B. Heintz, C. Farwell, L. Hu, F. S. Kinnaman, S. Yvon-Lewis, M. Du, E. W. Chan, F. G. Tigreros, C. J. Villanueva, Propane Respiration Jump-Starts Microbial Response to a Deep Oil Spill, Science 330 (6001) (2010) 208–211. doi:10.1126/science.1196830.

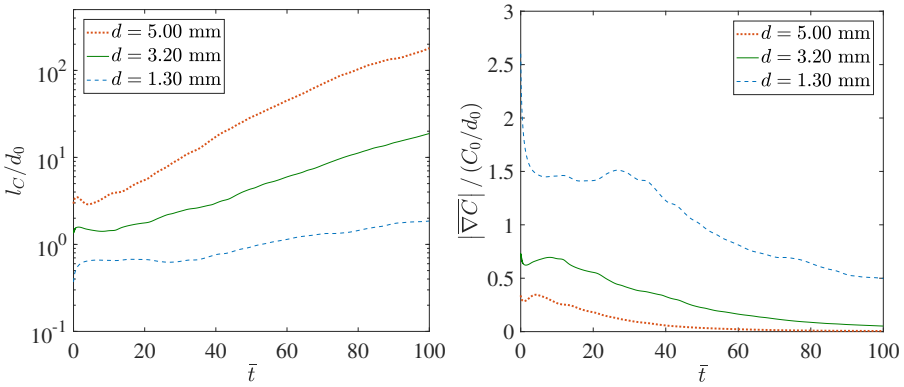

Figure 12: (Color online) (a) Time evolution of the nutrient heterogeneity length-scale l_C normalized by the drop diameter $d_0 = 0.13$ cm, for the background flows corresponding to different drop diameters, d. (b) Time evolution of the volume-averaged nutrient gradient $|\nabla C|$ normalized by a reference gradient C_0/l_{ref}, for the background flows corresponding to different drop diameters, d. The other parameters are: $\alpha_C = 1\text{x}10^{-8}$ cm^{3}s^{-1}cell^{-1}; $\beta_C = 40.0$ μMcm^{-1}s; $V_s = 100$ μm/s; $D_m = D_b = 5\text{x}10^{-4}$ cm^2/s; $C_0 = 25$ μM; $B_0 = 1.5\text{x}10^5$ cells/cm^3.

[3] R. M. Atlas, T. C. Hazen, Oil Biodegradation and Bioremediation: A Tale of the Two Worst Spills in U.S. History, Environmental Science & Technology (16) (2011) 6709–6715. doi:10.1021/es2013227.

[4] E. A. Dubinsky, M. E. Conrad, R. Chakraborty, M. Bill, S. E. Borglin, J. T. Hollibaugh, O. U. Mason, Y. M. Piceno, F. C. Reid, W. T. Stringfellow, L. M. Tom, T. C. Hazen, G. L. Andersen, Succession of Hydrocarbon-Degrading Bacteria in the Aftermath of the Deepwater Horizon Oil Spill in the Gulf of Mexico, Environmental Science & Technology 47 (19) (2013) 10860–10867. doi:10.1021/es401676y.

[5] T. B. Ryerson, R. Camilli, J. D. Kessler, E. B. Kujawinski, C. M. Reddy, D. L. Valentine, E. Atlas, D. R. Blake, J. de Gouw, S. Meinardi, D. D. Parrish, J. Peischl, J. S. Seewald, C. Warneke, Chemical data quantify Deepwater Horizon hydrocarbon flow rate and environmental distribution,

Proceedings of the National Academy of Sciences (50) (2012) 20246–20253. doi:10.1073/pnas.1110564109.

[6] B. Bunner, G. Tryggvason, Dynamics of homogeneous bubbly flows Part 1. Rise velocity and microstructure of the bubbles, Journal of Fluid Mechanics 466. doi:10.1017/S0022112002001179.

[7] B. Bunner, G. Tryggvason, Dynamics of homogeneous bubbly flows Part 2. Velocity fluctuations, Journal of Fluid Mechanics 466. doi:10.1017/S0022112002001180.

[8] S. Dabiri, A. Doostmohammadi, M. Bayareh, A. Ardekani, Rising motion of a swarm of drops in a linearly stratified fluid, International Journal of Multiphase Flow 69 (2015) 8–17. doi:10.1016/j.ijmultiphaseflow.2014.10.010.

[9] F. Risso, Agitation, Mixing, and Transfers Induced by Bubbles, Annual Review of Fluid Mechanics 50 (1) (2018) annurev–fluid–122316–045003. doi:10.1146/annurev-fluid-122316-045003.
URL http://www.annualreviews.org/doi/10.1146/annurev-fluid-122316-045003

[10] H. C. Berg, D. A. Brown, Chemotaxis in Escherichia coli analysed by Three-dimensional Tracking, Nature 239 (1972) 500–504.

[11] J. R. Taylor, R. Stocker, Trade-Offs of Chemotactic Foraging in Turbulent Water, Science 338 (6107) (2012) 675–679. doi:10.1126/science.1219417.

[12] G. A. Jackson, Seascapes: the world of aquatic organisms as determined by their particulate natures, Journal of Experimental Biology 215 (6) (2012) 1017–1030. doi:10.1242/jeb.059105.
URL http://jeb.biologists.org/cgi/doi/10.1242/jeb.059105

[13] S. O. Unverdi, G. Tryggvason, A front-tracking method for viscous, incompressible, multi-fluid flows, Journal of Computational Physics 100 (1) (1992) 25–37. doi:10.1016/0021-9991(92)90307-K.

[14] G. Tryggvason, B. Bunner, A. Esmaeeli, D. Juric, N. Al-Rawahi, W. Tauber, J. Han, S. Nas, Y.-J. Jan, A Front-Tracking Method for the Computations of Multiphase Flow, Journal of Computational Physics 169 (2) (2001) 708–759. doi:10.1006/jcph.2001.6726.

[15] D. Saintillan, M. J. Shelley, Theory of Active Suspensions, Springer, 2015, pp. 319–355. doi:10.1007/978-1-4939-2065-5_9.
URL http://link.springer.com/10.1007/978-1-4939-2065-5{_}9

[16] T. J. Pedley, N. A. Hill, J. O. Kessler, The growth of bioconvection patterns in a uniform suspension of gyrotactic micro-organisms, Journal of Fluid Mechanics 195 (-1) (1988) 223. doi:10.1017/S0022112088002393.
URL http://www.journals.cambridge.org/abstract{_}S0022112088002393

[17] A. Karimi, A. M. Ardekani, Gyrotactic bioconvection at pycnoclines, Journal of Fluid Mechanics 733 (2013) 245–267. doi:10.1017/jfm.2013.415.

[18] R. Bearon, Modelling Run-and-Tumble Chemotaxis in a Shear Flow, Bulletin of Mathematical Biology 62 (4) (2000) 775–791. doi:10.1006/bulm.2000.0178.

[19] K. C. Chen, R. M. Ford, P. T. Cummings, Cell balance equation for chemotactic bacteria with a biphasic tumbling frequency, Journal of Mathematical Biology 47 (6) (2003) 518–546. doi:10.1007/s00285-003-0216-8.

[20] E. F. Keller, L. A. Segel, Model for Chemotaxis, Journal of Theoretical Biology 30 (1971) 225–234.

[21] R. Thar, M. Kuhl, Bacteria are not too small for spatial sensing of chemical gradients: An experimental evidence, Proceedings of the National Academy of Sciences 100 (10) (2003) 5748–5753. doi:10.1073/pnas.1030795100.

[22] P. A. Iglesias, P. N. Devreotes, Navigating through models of chemotaxis, Current Opinion in Cell Biology 20 (1) (2008) 35–40. doi:10.1016/j.ceb.2007.11.011.

[23] J. Taktikos, V. Zaburdaev, H. Stark, Modeling a self-propelled autochemotactic walker, Physical Review E 84 (4). doi:10.1103/physreve.84.041924.

[24] J. Taktikos, V. Zaburdaev, H. Stark, Collective dynamics of model microorganisms with chemotactic signaling, Physical Review E 85 (5) (2012) 051901. doi:10.1103/PhysRevE.85.051901.

[25] M. M. Hopkins, L. J. Fauci, A computational model of the collective fluid dynamics of motile micro-organisms, Journal of Fluid Mechanics 455. doi:10.1017/S0022112001007339.

[26] E. Lushi, R. E. Goldstein, M. J. Shelley, Auto-chemotactic micro-swimmer suspensions: modeling, analysis and simulationsarXiv:1310.7614.

[27] R. Watteaux, R. Stocker, J. R. Taylor, Sensitivity of the rate of nutrient uptake by chemotactic bacteria to physical and biological parameters in a turbulent environment, Journal of Theoretical Biology 387 (2015) 120–135. doi:10.1016/j.jtbi.2015.08.006.

[28] A. J. Chorin, Numerical solution of the Navier-Stokes equations, Mathematics of Computation 22 (1968) 745–762.

[29] M. Bayareh, A. Doostmohammadi, S. Dabiri, A. M. Ardekani, On the rising motion of a drop in stratified fluids, Physics of Fluids 25 (10) (2013) 103302. doi:10.1063/1.4823724.

[30] B. Leonard, A stable and accurate convective modelling procedure based on quadratic upstream interpolation, Computer Methods in Applied Mechanics and Engineering 19 (1) (1979) 59–98. doi:10.1016/0045-7825(79)90034-3.

[31] C. S. Peskin, The immersed boundary method, Acta Numerica 11. doi:10.1017/S0962492902000077.

[32] B. Kubrak, H. Herlina, F. Greve, J. Wissink, Low-diffusivity scalar transport using a WENO scheme and dual meshing, Journal of Computational Physics 240 (2013) 158–173. doi:10.1016/j.jcp.2012.12.039.

[33] U. Ascher, L. Petzold, Computer Methods for Ordinary Differential Equations and Differential-Algebraic Equations, Society for Industrial and Applied Mathematics, 1998.

[34] L. Karp-Boss, E. Boss, P. A. Jumars, Nutrient fluxes to planktonic osmotrophs in the presence of fluid motion, Oceanography and Marine Biology: an Annual Review 34 (1996) 71–107.

[35] W. M. Durham, E. Climent, M. Barry, F. De Lillo, G. Boffetta, M. Cencini, R. Stocker, Turbulence drives microscale patches of motile phytoplankton, Nature Communications 4 (2013) 1–7. doi:10.1038/ncomms3148.
URL http://www.nature.com/doifinder/10.1038/ncomms3148

[36] C. B. Paris, M. L. Hénaff, Z. M. Aman, A. Subramaniam, J. Helgers, D.-P. Wang, V. H. Kourafalou, A. Srinivasan, Evolution of the Macondo Well Blowout: Simulating the Effects of the Circulation and Synthetic Dispersants on the Subsea Oil Transport, Environmental Science & Technology 46 (24) (2012) 13293–13302. doi:10.1021/es303197h.
URL http://pubs.acs.org/doi/abs/10.1021/es303197h

[37] P. J. Brandvik, Ø. Johansen, F. Leirvik, U. Farooq, P. S. Daling, Droplet breakup in subsurface oil releases Part 1: Experimental study of droplet breakup and effectiveness of dispersant injection, Marine Pollution Bulletin 73 (1) (2013) 319–326. doi:10.1016/j.marpolbul.2013.05.020.
URL http://linkinghub.elsevier.com/retrieve/pii/S0025326X13002671

[38] Ø. Johansen, P. J. Brandvik, U. Farooq, Droplet breakup in subsea oil releases Part 2: Predictions of droplet size distributions with and without injection of chemical dispersants, Marine Pollution Bulletin 73 (1) (2013) 327–335. doi:10.1016/j.marpolbul.2013.04.012.
URL http://linkinghub.elsevier.com/retrieve/pii/S0025326X1300194X

[39] E. W. North, E. E. Adams, A. E. Thessen, Z. Schlag, R. He, S. A. Socolofsky, S. M. Masutani, S. D. Peckham, The influence of droplet size and biodegradation on the transport of subsurface oil droplets during the Deepwater Horizon spill: a model sensitivity study, Environmental Research Letters 10 (2) (2015) 024016. doi:10.1088/1748-9326/10/2/024016.
URL http://stacks.iop.org/1748-9326/10/i=2/a=024016?key=crossref.14b99ec1a39331aa45a0cb87477ff4b8

[40] R. Stocker, J. R. Seymour, Ecology and Physics of Bacterial Chemotaxis in the Ocean, Microbiology and Molecular Biology Reviews 76 (4) (2012) 792–812. doi:10.1128/MMBR.00029-12.

[41] H. C. Berg, Random Walks in Biology., 2nd Edition, Princeton, Princeton, New Jersey, 1993.

[42] T. Kiørboe, A mechanistic approach to plankton ecology, Princeton University Press, 2008.

[43] K. Son, J. S. Guasto, R. Stocker, Bacteria can exploit a flagellar buckling instability to change direction, Nature Physics 9 (8) (2013) 494–498. doi:10.1038/nphys2676.
URL http://www.nature.com/doifinder/10.1038/nphys2676

[44] E. L. Cussler, Diffusion: Mass Transfer in Fluid Systems, 2nd Edition, Cambridge University Press, New York, NY, 1997.